Generation and propagation of high-order harmonics in a rapidly ionizing medium

S. C. Rae and K. Burnett
Clarendon Laboratory, Department of Physics, University of Oxford, Oxford OX1 3PU, United Kingdom

J. Cooper
Joint Institute for Laboratory Astrophysics, University of Colorado, Boulder, Colorado 80309-0440
(Received 19 July 1993; revised manuscript received 25 April 1994)

We present the results from simulations of harmonic generation using intense ultrashort laser pulses, both for single atoms and in an extended gaseous medium. Using a windowing technique on the single-atom spectrum, we show that the highest-order harmonics are generated simultaneously with rapid ionization, and that these harmonics have a phase dependence which is consistent with a quasiclassical tunneling model. By solving the atomic dynamics simultaneously with the propagation equations, we have obtained spectra that directly show the effects of phase mismatching and blueshifting produced by an ionizing medium. At experimental pressures, the plasma-induced phase mismatch is only important for the highest-order harmonics near the plateau cutoff. All harmonic orders, however, are seen to be blueshifted, by an amount consistent with a blueshifting of the fundamental as it propagates through the ionizing medium.

PACS number(s): 42.65.Ky, 52.40.Db, 32.80.Rm

I. INTRODUCTION

If an intense ultrashort laser pulse is weakly focused into a rare-gas jet, high-order odd harmonics of the incident radiation can be produced [1–7]. Theoretically, there are two distinct aspects to this problem: the single-atom process in which the harmonics are generated, and the way in which the harmonics propagate through the medium. A complete theoretical model of harmonic generation should give equal consideration to both of these aspects. The most extensive modeling work to date, by L'Huillier and co-workers, uses a two-dimensional (2D) slowly-varying-envelope (SVE) treatment of the propagation and direct numerical solution of the 3D Schrödinger equation to obtain the atomic dynamics [8]. When the rate of ionization is low (less than about 1% per cycle) and the laser pulse is relatively long ($\gg$1 ps) such a method is highly successful at quantitatively reproducing experimental results.

Developments in short-pulse laser technology, particularly the advent of Ti:sapphire [9,10] and Cr:LiSAF [11] as amplification media, have moved harmonic generation experiments into a different regime. With pulses as short as 100 fs, a SVE approximation is no longer valid. The dipole moment cannot be calculated initially at a number of fixed intensities and then used as an intensity-dependent function in a propagation code, but instead the atomic response must be calculated for the pulse as a whole. A self-consistent approach is necessary, in which the atomic dynamics and propagation are considered simultaneously.

In this paper we describe numerical simulations of harmonic generation and propagation, outside the SVE regime, using a 1D Schrödinger equation for the atomic dynamics and plane wave propagation. Such simulations cannot, of course, address issues related to focusing and geometric phase matching, so are only physically appropriate to situations where the confocal parameter is very large. The model has been specifically designed for investigating the effects of phase mismatching and blueshifting due to free electrons. These effects arise because the intense laser pulse partially or completely ionizes the gaseous medium. The time varying refractive index in the plasma gives rise to a blueshifting of the fundamental and harmonics, and dispersion in the resultant plasma may reduce the coherence and thus the overall generation efficiency of the harmonics. We wish to find out how serious these effects are, and whether they affect all harmonic orders in a similar way.

In the first half of the paper, we address single-atom spectra, in particular examining the time dependence of harmonic emission on the time scale of the laser pulse and also on a time scale within a laser cycle. Following this, we will describe the incorporation of the model atom into the equation for plane wave propagation, and show how the ionizing medium can affect the overall harmonic spectrum, both in terms of reduced conversion efficiency and plasma-induced blueshifting of the harmonics.

II. SINGLE-ATOM CALCULATIONS

A. Atomic dynamics

In our model, the atomic dynamics are obtained by numerically solving the 1D Schrödinger equation in the Kramers-Henneberger (KH) frame. The dynamical behavior of the 1D model atom has been extensively studied in the past by Eberly, Su, and Javanainen [12], and others [13,14]. In atomic units, the 1D Schrödinger equation can be written

$$i\frac{\partial\psi}{\partial t}(x,t) = -\frac{1}{2}\frac{\partial^2\psi}{\partial x^2}(x,t) + V(x+\alpha(t))\psi(x,t)\ , \quad (1)$$

 ©1994 The American Physical Society

where the potential is of the form

$$V(x) = \frac{-1}{\sqrt{\beta + x^2}} . \quad (2)$$

The parameter $\alpha(t)$ represents the time-dependent displacement of the KH frame, and has an amplitude given by $\alpha_0 = E_0/\omega^2$, where E_0 is the amplitude of the laser electric field and ω is the angular frequency. Note that we use atomic units throughout this paper, except where noted.

The scaling parameter β can be adjusted to match the ionization potential of the model atom to that of any real atom. In the present case, we choose $\beta = 1.414$, which gives an ionization potential of 15.76 eV, equal to that of argon. Figure 1 shows the potential for this case, together with the energies of the bound states. The total number of bound states depends upon the size of the numerical grid, but in the present case is typically 15.

As in our previous studies [15], we start with the wave function in the ground state of the potential. Equation (1) is solved numerically using a semi-implicit Crank-Nicolson technique [16], and the single-atom spectrum is obtained from a Fourier transform of the dipole acceleration [17],

$$a(t) = \left\langle \psi(t) \left| \frac{-\partial V}{\partial x} \right| \psi(t) \right\rangle + E(t) , \quad (3)$$

recorded over the entire laser pulse.

The size of the grid is determined by the laser intensity and frequency, and typically must be somewhat greater than $2\alpha_0$. The time step and space step are found by trial and error, and represent compromises between computational speed and numerical accuracy. For the studies here, we have generally used a grid of 800 points with spacing 0.2 a.u., and 400 time steps per laser cycle. The laser pulse is 100 cycles long, with a sine-squared field envelope of the form

$$E(t) = E_0 \sin\omega t \sin^2\left(\frac{\pi t}{\tau}\right) . \quad (4)$$

The frequency is 0.056 55 a.u., so these conditions correspond to a 100 fs full width at half maximum laser pulse of wavelength 800 nm. There are absorbing regions of width 200 points at the edges of the grid, with a mask of $\cos^{1/8}$ shape, as used previously by Krause, Schafer, and Kulander [18]. The absorbing region must be so large because during rapid ionization parts of the wave function will reach the edges of the grid moving with a very high velocity, and even a small amount of reflection can significantly alter the resultant spectrum. Since any part of the wave function which reaches the edges of the grid during the calculation disappears, the degree of ionization Z can be estimated by calculating the norm of the wave function $\langle\psi|\psi\rangle$ which remains.

Figure 2 shows some results from the 1D model for peak laser intensities of 5.5×10^{13}, 1.2×10^{14}, and 2.2×10^{14} W/cm^2. Note that for these spectra the fundamental term in $E(t)$ has been omitted from the dipole acceleration expression in Eq. (3) for simplicity. The harmonic spectra show a characteristic plateau region followed by a steep drop in conversion efficiency beyond a cutoff point. Both the number of harmonics and the intensity of the plateau harmonics increase with laser intensity, until an intensity is reached where the atom ionizes rapidly in the leading edge of the laser pulse.

The position of the cutoff corresponds closely to that predicted by a simple quasiclassical tunneling theory developed by Corkum and others [19,20], which gives the cutoff harmonic q_c as

$$q_c \simeq \mathcal{E}_i + 3\mathcal{E}_q . \quad (5)$$

Here $\mathcal{E}_i$ is the ionization potential and $\mathcal{E}_q = E_0/4\omega^2$ is the quiver or ponderomotive energy. For the conditions of Fig. 2, Eq. (5) predicts that $q_c \simeq 17$, 25, and 37, in good agreement with the actual spectra. It should be noted that under typical experimental conditions, propagation

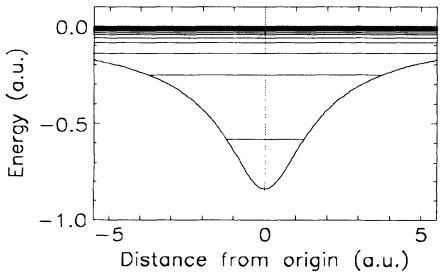

FIG. 1. Potential used in the 1D model argon atom, with a ground state binding energy of 15.76 eV and 15 bound states in total.

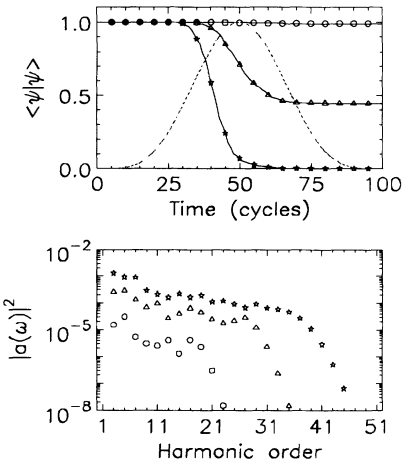

FIG. 2. Degree of ionization as a function of time (top) and harmonic spectra (bottom) for a 1D model argon atom subjected to a 100-cycle, 800-nm laser pulse of peak intensity 5.5×10^{13} W/cm^2 (circles), 1.2×10^{14} W/cm^2 (triangles), and 2.2×10^{14} W/cm^2 (stars). The dotted line in the top figure shows the laser pulse envelope.

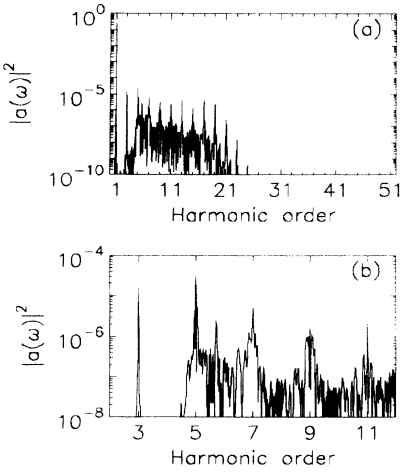

FIG. 3. (a) Harmonic spectrum for a 1D model argon atom subjected to a 100-cycle, 800-nm laser pulse of peak intensity 5.5×10^{13} W/cm^2, and (b) detail of full spectrum.

effects due to the focusing geometry act to reduce the cutoff and Eq. (5) is no longer strictly appropriate [21].

In Fig. 2 we have only shown the positions of the harmonic peaks, but there is considerable structure beneath the peaks, as Figs. 3 and 4 show for intensities of 5.5×10^{13} and 2.2×10^{14} W/cm^2, respectively. The relatively high background intensity is largely due to the short-pulse duration and rapidly varying envelope. Simulation conditions which use a significantly longer pulse [15], or a ramped turn on followed a period of constant laser intensity [18] typically result in a much cleaner spectrum than those shown here. There are also numerous smaller peaks off the exact harmonic positions, which are probably due to transitions between dynamically Stark-shifted levels in the strongly driven atom. These peaks become more prominent as the intensity is raised, which can be clearly seen in the comparison of Figs. 3 and 4. The secondary peaks, however, are not coherent with the driving field and would not phase match successfully in an extended medium, which probably explains why experimental spectra are generally free of such spurious peaks.

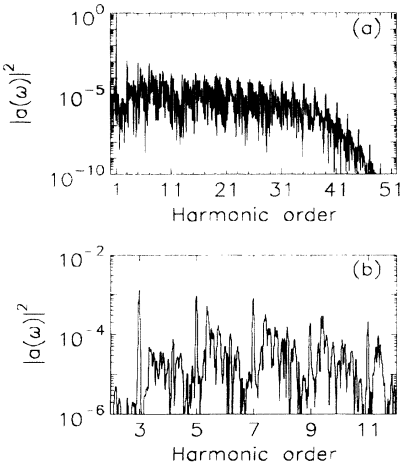

FIG. 4. (a) Harmonic spectrum for a 1D model argon atom subjected to a 100-cycle, 800-nm laser pulse of peak intensity 2.2×10^{14} W/cm^2, and (b) detail of full spectrum.

B. Time-dependent spectra

A crucial issue for phase mismatching and blueshifting due to free electrons is the relative timing of ionization and harmonic generation. If the bulk of the harmonics are generated before the period of rapid ionization, then they will propagate through an essentially neutral medium, but any harmonics generated during the ionization process will be subject to dispersion and blueshifting.

The simplest way to investigate this issue is to construct a time-dependent harmonic spectrum. This can be done in a simple way by multiplying the dipole acceleration by a narrow temporal window function before taking a Fourier transform, a procedure closely related to power spectrum estimation [22]. We have used a triangular window of width ten laser cycles, which can be moved through the pulse to map out the time dependence of the harmonic emission. Figure 5 shows a set of windowed spectra for the same conditions as Fig. 4.

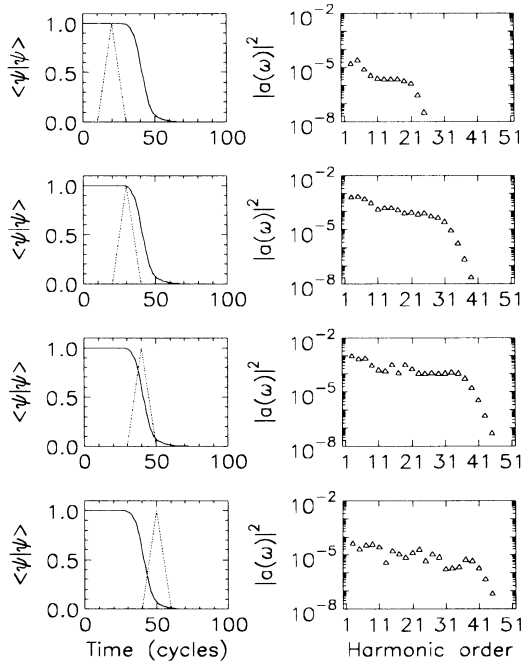

FIG. 5. Harmonic spectra obtained under the same conditions as Fig. 4, but with a ten-cycle triangular window applied to the dipole acceleration data. The left-hand figure in each case shows the position of the window (dotted line) compared to the time-dependent degree of ionization (solid line).

a 100-cycle, 800-nm pulse with peak intensity 2.2×10^{14} W/cm^2. The spectra clearly show that the harmonics at the plateau cutoff are produced concurrently with the period of rapid ionization, occurring in this case just before the peak of the laser pulse is reached. The low-order harmonics appear to be produced slightly earlier in the laser pulse as well as during the period of rapid ionization.

The duration of emission can be seen more clearly in Fig. 6, where we show the ionization rate as a function of time, together with the normalized intensities of the fundamental, the 3rd harmonic and the 37th harmonic. The peak in emission for the 3rd harmonic occurs slightly before the peak for the 37th, although the rate of ionization at peak emission is similar in the two cases. The emission duration for the 3rd harmonic is noticeably longer than for the 37th, with both being significantly less than the laser pulse duration itself.

The technique of windowing the dipole acceleration before performing a Fourier transform can also be used to investigate the phase dependence of the harmonic emission. This is of interest because the quasiclassical tunneling model referred to earlier [19,20] makes specific predictions about the times during a laser cycle at which the highest-order harmonics are generated. Briefly, the model assumes that an essentially free electron is produced by tunneling through the suppressed potential barrier, and that this electron then evolves classically under the influence of the laser field only. For particular values of the initial phase at ionization, the electron will traverse a path which brings it back to the origin, where it can again interact with the nucleus. The maximum kinetic energy of the electron upon its return, relative to the ground state energy of the atom, sets an upper limit on the energy of the photon which can be emitted, and hence the position of the harmonic cutoff.

After tunneling through the potential barrier, the electron's motion (assuming linearly-polarized light $E = E_0 \sin \omega t$) is given by

$$x = x_q(-\sin \omega t) + v_0 t + x_0 \ , \tag{6}$$

$$v = v_q(-\cos \omega t) + v_0 \ , \tag{7}$$

where $v_q = E_0/\omega$ is the quiver velocity and $x_q = v_q/\omega$ is the quiver amplitude. The initial conditions v_0 and x_0 can be calculated by assuming that $v = x = 0$ at the time of tunneling. The maximum return velocity, which defines the cutoff energy in Eq. (5), occurs for an electron tunneling out at $\omega t = \phi \simeq 107°$ or 287°, and returning to the vicinity of the nucleus at $\phi \simeq 345°$ or 165°. This would suggest, if the model accurately describes the physical situation, that the emission of the highest-order harmonics should peak at the phases of the laser cycle corresponding to those return times, in other words, just before the zero crossings of the electric field.

As we are specifically interested in the harmonic emission on a time scale less than a laser cycle, it is necessary to use a window on the dipole acceleration of width $\tau \ll \tau_0 = 2\pi/\omega$. Using such a narrow window means that individual harmonic peaks will no longer be resolved in the spectrum. A window of width $\tau = \tau_0/10$ will not be able to resolve features in the spectrum smaller than about ten photon energies in size. Figure 7 illustrates this point, showing the power spectrum obtained for the conditions of Fig. 4, with a $\tau_0/10$ window centered at a time 40 cycles into the laser pulse. All traces of harmonic peaks have disappeared, although it is still the

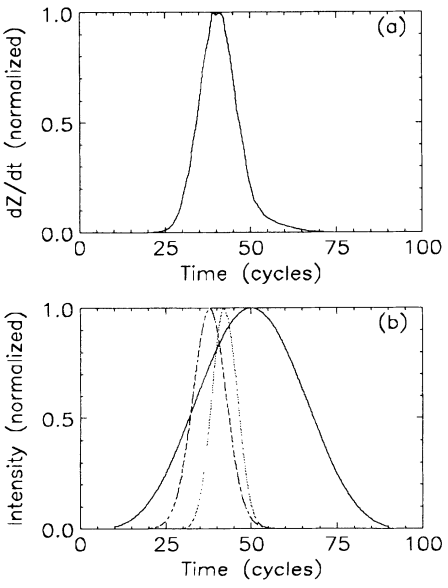

FIG. 6. (a) Ionization rate as a function of time for the conditions of Fig. 4, and (b) normalized intensities of the fundamental (solid line), 3rd harmonic (dashed line), and 37th harmonic (dotted line). Harmonic intensities have been obtained by scanning a ten-cycle triangular window across the full dipole acceleration data.

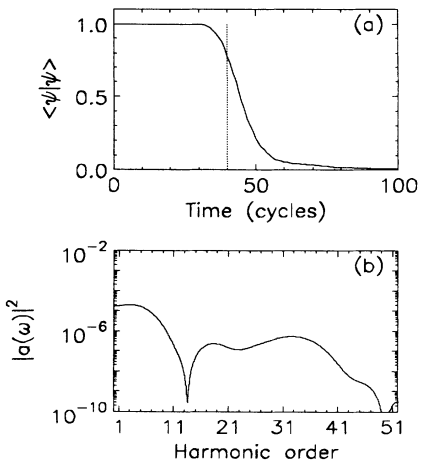

FIG. 7. (a) Degree of ionization as a function of time for the conditions of Fig. 4, together with a triangular window of width $\tau_0/10$ applied to the dipole acceleration data, and (b) resultant power spectrum.

case that the spectrum accurately represents the power radiated into specific frequency ranges. As the resolution is effectively 10ω, it makes sense to divide the windowed spectrum into bins of width 10ω, and integrate across each bin to obtain an average value.

We have used such a technique to compare the phase dependence of low-order and high-order harmonic emission for the conditions of Fig. 4. At two different times in the laser pulse, after 20 and 40 cycles, we have scanned a $\tau_0/10$ window across a single laser cycle to obtain the phase dependence of the harmonic emission into various orders. The results are plotted in Fig. 8, where the two curves in each case correspond to the average intensity in the frequency ranges $(0\text{–}10)\omega$ (low-order harmonics) and $(30\text{–}40)\omega$ (high-order harmonics). In Fig. 8(a), both low-order and high-order harmonics show the same phase dependence. The emission into all harmonic orders is seen to peak at $\phi \simeq \pm 90°$ (where the field is a maximum) and pass through a minimum close to $\phi \simeq 0°$, 180° (where the field is zero). Moving further into the pulse, from Fig. 8(a) to Fig. 8(b), there is little change in the behavior of the low-order harmonics, but the high-order harmonics increase significantly in intensity and undergo a dramatic phase shift, so that at this time the low-order and high-order harmonics are produced almost exactly 180° out of phase. Emission into the high-order harmonics now peaks close to $\phi = 0°$ and 180°, as predicted by the quasiclassical tunneling model. The plateau region of harmonics in the range $(10\text{–}30)\omega$, not shown in Fig. 8, displays a fairly flat phase dependence, without the clear structure observed with the low-order or high-order harmonics.

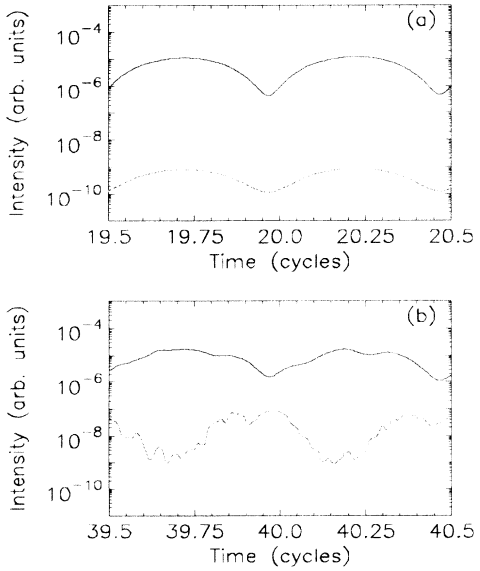

FIG. 8. Time dependence of harmonic emission for the conditions of Fig. 4, obtained using a window of width $\tau_0/10$, scanned over one cycle at (a) 20 cycles into the pulse, and (b) 40 cycles into the pulse. In each case the solid line represents the average intensity in the frequency range $(0\text{–}10)\omega$, and the dotted line represents the average intensity in the frequency range $(30\text{–}40)\omega$.

The quasiclassical model is only expected to apply in the tunneling regime, where the adiabaticity parameter, γ, defined by

$$\gamma = (\mathcal{E}_i/2\mathcal{E}_q)^{1/2} , \tag{8}$$

is less than unity. For the conditions of Fig. 8, the adiabaticity parameter takes the values $\gamma = 2.2$ at $t = 20$ cycles and $\gamma = 0.84$ at $t = 40$ cycles. Thus, we would only expect the tunneling conditions to be met near the peak of the laser pulse, which in this case is where the high-order harmonics are being generated. Through its dependence on the quiver energy, γ scales as ω/E, and thus for a given electric field strength we would expect the tunneling behavior to be more pronounced for longer laser wavelengths.

The phase-dependent emission observed is strong evidence that two different mechanisms are involved in harmonic generation in strongly-driven atoms. One mechanism, responsible for all low-order harmonics, appears to be a single-step mechanism which occurs close to the core and thus peaks when the electric field of the laser is at a maximum. The other mechanism generates the high-order harmonics during rapid ionization in the tunneling regime, and shows a quite different phase dependence, with emission peaking near the field crossing points. In the tunneling regime, plateau harmonics can be produced by combination of the two mechanisms and thus show a flat phase dependence.

III. PROPAGATION EFFECTS

A. Propagation model

The propagation part of our model is similar to that used previously to investigate the phase matching of harmonics produced in the extreme tunneling ionization limit [23]. The wave equation for the propagation of a plane wave, linearly polarized field $E(z,t)$ can be written

$$\frac{\partial^2 E}{\partial z^2} - \frac{1}{c^2}\frac{\partial^2 E}{\partial t^2} - \mu_0 \frac{\partial J}{\partial t} = 0 , \tag{9}$$

where J is the plasma current. The time derivative of J is directly proportional to the single atom dipole acceleration,

$$\frac{\partial}{\partial t} J(z,t) = N(z)\, a(z,t) , \tag{10}$$

where $N(z)$ is the density profile of the atoms.

Equation (9) can be solved numerically using an explicit finite-difference technique [16]. We start with the laser pulse in a vacuum region, and then propagate the pulse through an interaction region containing a large number of 1D model atoms. A Fourier transform of the laser pulse exiting the interaction region yields the harmonic spectrum. We use a laser pulse, as in the previous section, of length 100 cycles, and a space step in the prop-

agation direction of 0.005λ, where λ is the vacuum laser wavelength. Computational restrictions limit the plasma region to just 50 atoms, and as the atoms are spaced by one grid point, this means that the total size of the plasma region is 0.25λ. As the laser pulse propagates through the plasma, the local field $E(z,t)$ at each grid point is used as the input to a separate 1D Schrödinger equation.

For phase matching considerations, the density-length product is the relevant parameter, and even though our interaction region is very short, we can increase the density in the model to reproduce the density-length products typically found in experiments. This scaling is valid as long as the density in the model remains well below the plasma critical density, at which point the generation of a reflected wave renders it invalid. For the present conditions, a practical upper limit on the density-length product is ~10 Torr over 1 mm. We should point out that this limitation is purely computational, and it is in principle possible to use the model with a much larger plasma interaction region and hence simulate significantly higher pressures. Because a sharp-edged plasma is more likely to generate reflections, the plasma density profile is also given a smooth sine-squared envelope.

Figure 9 shows a comparison of a single atom spectrum [from Fig. 4(a)] and a propagated spectrum, for a laser intensity of 2.2×10^{14} W/cm^2, and a propagated density-length product of 5 Torr over 1 mm. The fundamental peak in Fig. 9(a) is much stronger than that in Fig. 4(a), because we have now included the term in $E(t)$ in the dipole acceleration expression in Eq. (3). The low-order harmonics in the propagated case are higher than the single-atom case because the power spectrum is strictly proportional to $\omega^2|a(\omega)|^2$ [17]. The propagated spectrum, which is the Fourier transform of the electric field, gives the true conversion efficiencies from the fundamental into the various harmonic orders. The peaks are considerably cleaner in the propagated case, because the incoherent off-harmonic peaks have been suppressed relative to the coherent harmonic peaks. For the present model, with only 50 atoms, the difference between N and N^2 is not so marked, but in a real physical system, the incoherent peaks would virtually disappear from the spectrum.

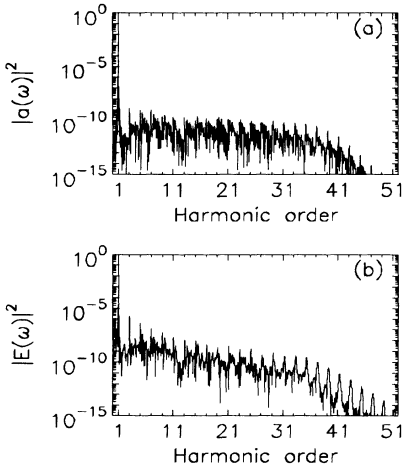

FIG. 9. Comparison of (a) the single-atom spectrum and (b) the propagated spectrum for a 50-atom model argon plasma and a 100-cycle, 800-nm laser pulse with peak intensity 2.2×10^{14} W/cm^2. The equivalent density-length product in (b) is 5 Torr over 1 mm.

B. Phase mismatching

Figure 10 shows the harmonic intensities for three propagated spectra with density-length products 0.1, 1, and 5 Torr over 1 mm, all for a laser intensity of 2.2×10^{14} W/cm^2. It can be seen that the absolute conversion efficiency into the plateau harmonics is around 10^{-10} at the highest pressures, and that the efficiency of harmonic generation appears to scale roughly as the square of the density, as expected for a coherent process. A better way to investigate the pressure dependence in detail is to choose a number of harmonic orders and plot the generation efficiency against pressure. This is done in Fig. 11 for the 3rd harmonic, the 13th (near the start of the plateau), and the 37th (near the cutoff). Dotted lines on this figure indicate a true N^2 dependence. While the 3rd harmonic appears to be relatively unaffected by phase mismatching, both the 13th and 37th harmonics are reduced in intensity at high pressures, attributable to dispersion in the ionizing medium.

Plasma dispersion is due to a difference in refractive indices for the fundamental and harmonic radiation. A coherence length L_c can be defined as the distance over which the mismatch is equal to 2π. For a singly ionized plasma, this is given (in SI units) by

$$L_c = \frac{4\pi c\epsilon_o m_e}{e^2}\,\frac{\omega}{N}\,\frac{q}{q^2-1}\,, \tag{11}$$

where N is the atomic density and q is the harmonic order. For propagation distances much less than L_c, the harmonic efficiency should scale as N^2, but at $L = L_c$,

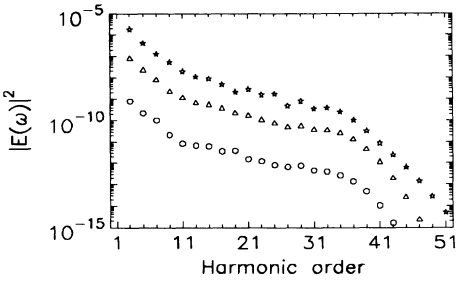

FIG. 10. Propagated harmonic spectra, showing peaks only, for a 50-atom model argon plasma and a 100-cycle, 800-nm laser pulse with peak intensity 2.2×10^{14} W/cm^2. The equivalent density-length products are 0.1 Torr (circles), 1 Torr (triangles), and 5 Torr (stars) over 1 mm.

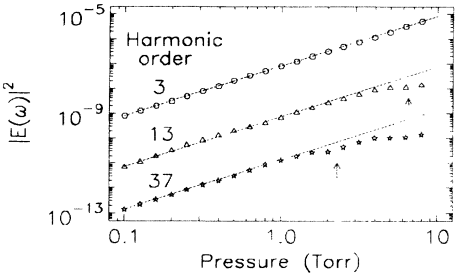

FIG. 11. Pressure dependence of selected harmonic intensities, for the same conditions as Fig. 10. The dotted lines indicate a true N^2 relationship, and the arrows mark the pressures at which the phase mismatch would be 2π for the 13th and 37th harmonics in a fully ionized plasma.

the efficiency passes through a minimum, and for $L \gg L_c$ the process becomes incoherent and the efficiency saturates.

In a previous study [23] in which harmonics were assumed to be generated by the tunneling ionization process itself (with no additional atomic dynamics), we found that all harmonic orders were generated at the same time in the pulse, corresponding to the period of maximum ionization rate. The harmonic efficiency as a function of pressure showed clear minima, associated with the phase mismatch equal to multiples of 2π. In the present case, assuming complete ionization, the pressures required to reach a phase mismatch of 2π for the 3rd, 13th, and 37th harmonics are 28, 6.5, and 2.3 Torr, respectively. These pressures, indicated by arrows for the latter two cases in Fig. 11, are those for which the relevant coherence length equals 1 mm. Deviations from the N^2 relationship do occur at around these pressures, although the complex ionization dynamics from the 1D atomic model prevent the observation of clear minima near the critical pressures as in the pure tunneling ionization case. The 3rd harmonic is virtually unaffected, but this would be expected even if it were generated in a fully ionized plasma at these pressures. Overall the effect of the free-electron phase mismatch on conversion efficiencies is fairly small, amounting to no more than one order of magnitude over the parameter range considered. However, because the conversion efficiencies for the higher harmonic orders are starting to saturate, the effect would become more severe if the pressure were increased further.

C. Plasma-induced blueshifting

Radiation which propagates through a medium with a time varying refractive index will be subject to frequency chirping. In harmonic generation at high intensities, the formation of a plasma during the laser pulse results in a decrease in the refractive index and hence a blueshifting of the fundamental and harmonics. Blueshifting of intense laser pulses in gases has been extensively studied experimentally and theoretically [24–27] and blueshifted harmonics have recently been observed by a number of groups [1,4].

In the simplest case, for an initial frequency ω propagating through a homogeneous medium of length L, the plasma-induced frequency shift can be written

$$\frac{\delta\omega}{\omega} = \frac{1}{2}\frac{\omega_p^2}{\omega^2}\frac{L}{c}\frac{dZ}{dt} . \tag{12}$$

Here ω_p is the plasma frequency for the fully ionized medium (in SI units, $\omega_p^2 = e^2 N_e/\epsilon_0 m_e$), c is the speed of light, and Z is the degree of ionization. Equation (12) assumes that the frequency is much greater than the plasma frequency, or in other words that the density is far below critical. The inverse scaling with frequency means that we would expect the fundamental to be more strongly blueshifted than the high-order harmonics. A straightforward application of Eq. (12) for a density of 5 Torr, interaction length of 1 mm, laser wavelength of 800 nm and ionization rate of $(50\ \text{fs})^{-1}$ gives $\delta\omega/\omega = 0.3\%$ for the fundamental, but only 0.02% for the 13th harmonic. Thus, any blueshifts observed on the harmonics probably arise from a blueshifted fundamental being up converted, rather than from a direct blueshifting of the harmonics themselves. Given this, all harmonic orders should show roughly the same blueshift in terms of $\delta\omega/\omega$.

In this section we will investigate the blueshifting observed in our simulations, for the same set of conditions as used previously, a 100-fs, 800-nm laser pulse of peak intensity 2.2×10^{14} W/cm^2, propagating through argon gas at various pressures. Figure 12 shows the spectrum of the fundamental, before and after propagation through a 1-mm length of 5-Torr gas. There is a slight broadening and overall blueshift of about 0.1%, but not as much as the 0.3% estimated earlier. This is because the ionization occurs rapidly over a relatively small fraction of the total pulse length, and most of the laser pulse, including the peak intensity, actually moves through a medium with an almost constant refractive index. The harmonics, however, are generated predominantly before the pulse peak, during the time of rapid ionization, so for these we should expect to see clearer evidence of blueshifting.

Figures 13, 14, and 15 show the profiles of the 3rd,

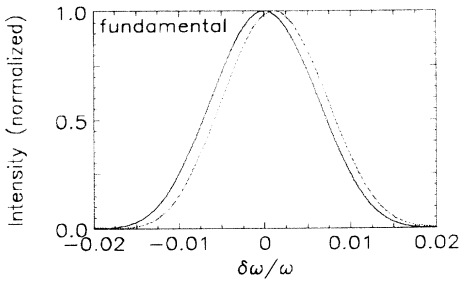

FIG. 12. Spectrum of the fundamental for a 100-cycle, 800-nm laser pulse with peak intensity 2.2×10^{14} W/cm^2 before (solid line) and after (dotted line) propagation through a 50-atom argon plasma with a density-length product of 5 Torr over 1 mm.

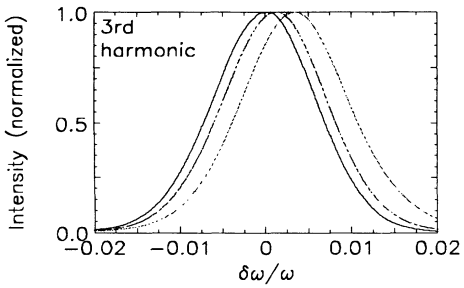

FIG. 13. Spectrum of the 3rd harmonic generated by a 100-cycle, 800-nm laser pulse with peak intensity 2.2×10^{14} W/cm^2 propagating through a 50-atom argon plasma with a density-length product of 0.1 Torr (solid line), 2 Torr (dashed line), and 5 Torr (dotted line) over 1 mm.

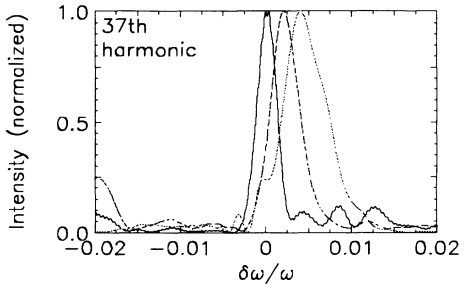

FIG. 15. Spectrum of the 37th harmonic generated by a 100-cycle, 800-nm laser pulse with peak intensity 2.2×10^{14} W/cm^2 propagating through a 50-atom argon plasma with a density-length product of 0.1 Torr (solid line), 2 Torr (dashed line), and 5 Torr (dotted line) over 1 mm.

13th, and 37th harmonics, for the same pulse conditions as Fig. 12, after propagation through 1 mm of argon at pressures of 0.1, 2, and 5 Torr. The lowest of these pressures effectively results in no blueshift, so the solid curve in each case can be used as a reference line shape. In the case of Fig. 15, the structure on the 37th harmonic at 0.1 Torr is not due to blueshifting but rather due partly to additional peaks in the atomic spectrum and partly to computational noise. The width of the unshifted line shape is governed mainly by the duration of the emission. If we assume as a rough estimate that the emission duration Δt is related to the frequency width $\Delta\omega$ by $\Delta t = 2\pi/\Delta\omega$, then the frequency widths observed correspond to approximate emission durations of 60, 50, and 30 fs for the 3rd, 13th, and 37th harmonics, respectively.

At higher pressures the harmonics all appear to be blueshifted by approximately the same amount in $\delta\omega/\omega$, confirming our earlier hypothesis about the shifts all arising from a shift in the fundamental. The shift also appears to be linear in the pressure, as predicted by Eq. (12). A noticeable feature is that in all cases the peak shifts noticeably in frequency, rather than remaining at the original frequency and merely broadening to the blue side. This would suggest that the emission into all harmonics occurs dominantly during the period of rapid ionization. If, on the other hand, emission occurred equally before ionization and during ionization, we would expect to see a peak broadened to the blue side but with some intensity remaining at the original center frequency.

Recent experimental work by Wahlström and coworkers [1] has shown that both blueshifted and blue-broadened harmonic line shapes can be observed. Harmonics in the plateau region are seen to be broadened, whereas those near the cutoff are purely shifted with little broadening. They postulate that this difference is due to the emission duration of the harmonics, with plateau harmonics being produced both early in the pulse and during the time of rapid ionization. The results from our simulations do not support this, however, as even for the 3rd harmonic we find the emission is strongly peaked during the rapid ionization period (see Fig. 6) and we observe an almost purely shifted line shape. We would suggest that the broadened line shapes observed by Wahlström and co-workers are a product of spatial, and not temporal, variation. In a focussed pulse the harmonics close to the cutoff will only be produced at the focal center. The plateau harmonics will also be generated at larger radial distances, where the ionization rate and the blueshift is less, and spatial averaging can lead in this case to a broadened line shape. The simulation results presented here, which explicitly assume plane-wave propagation, unfortunately cannot address the issue of spatial averaging.

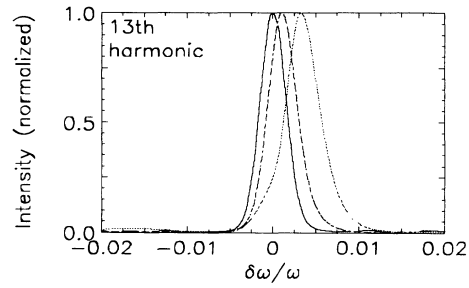

FIG. 14. Spectrum of the 13th harmonic generated by a 100-cycle, 800-nm laser pulse with peak intensity 2.2×10^{14} W/cm^2 propagating through a 50-atom argon plasma with a density-length product of 0.1 Torr (solid line), 2 Torr (dashed line), and 5 Torr (dotted line) over 1 mm.

IV. CONCLUSION

We have performed calculations of harmonic generation in an extended medium by solving the equations for the atomic dynamics and the propagation simultaneously. This is the first time, to our knowledge, that absolute efficiencies and propagated spectra have been obtained outside the SVE approximation. Our study has highlighted the fact that in an intense ultrashort laser pulse most of the harmonic radiation is generated during the period of rapid ionization, which may not coincide with the peak of the laser pulse. There appear to be

two mechanisms for harmonic generation with different phase characteristics, and we have observed that for high-order harmonics, generated in the tunneling regime, the phase dependence is correctly given by a simple quasi-classical model. The production of a plasma during the harmonic generation process has two effects, a reduction in the conversion efficiency of the high-order harmonics due to phase mismatching, and a blueshifting of the harmonics due to a time varying refractive index. All harmonic orders appear to be blueshifted in a similar way, suggesting that the blueshift originates with a blueshifted fundamental. Linewidths are not appreciably broadened by the blueshifting process, and recent experimental results showing broadened harmonics are most likely the result of spatial averaging rather than temporal effects.

ACKNOWLEDGMENT

This work is part of a program supported by the Science and Engineering Research Council of the United Kingdom.

[1] C.-G. Wahlström, J. Larsson, A. Persson, T. Starczewski, S. Svanberg, P. Salières, P. Balcou, and A. L'Huillier, Phys. Rev. A **48**, 4709 (1993).
[2] J. W. G. Tisch, R. A. Smith, J. E. Muffett, M. Ciarrocca, J. P. Marangos, and M. H. R. Hutchinson, Phys. Rev. A **49**, R28 (1994).
[3] A. L'Huillier and P. Balcou, Phys. Rev. Lett. **70**, 774 (1993).
[4] J. J. Macklin, J. D. Kmetec, and C. L. Gordon III, Phys. Rev. Lett. **70**, 766 (1993).
[5] K. Miyazaki and H. Sakai, J. Phys. B **25**, L83 (1992).
[6] J. K. Crane, M. D. Perry, S. Herman, and R. W. Falcone, Opt. Lett. **17**, 1256 (1992).
[7] N. Sarukura, K. Hata, T. Adachi, R. Nodomi, M. Watanabe, and S. Watanabe, Phys. Rev. A **43**, 1669 (1991).
[8] A. L'Huillier, K. J. Schafer, and K. C. Kulander, J. Phys. B **24**, 3315 (1991); A. L'Huillier, K. J. Schafer, and K. C. Kulander, Phys. Rev. Lett. **66**, 2200 (1991); A. L'Huillier, P. Balcou, S. Candel, K. J. Schafer, and K. C. Kulander, Phys. Rev. A **46**, 2778 (1992).
[9] J. D. Kmetec, J. J. Macklin, and J. F. Young, Opt. Lett. **16**, 1001 (1991).
[10] A. Sullivan, H. Hamster, H. C. Kapteyn, S. Gordon, W. White, H. Nathel, R. J. Blair, and R. W. Falcone, Opt. Lett. **16**, 1406 (1991).
[11] T. Ditmire and M. D. Perry, Opt. Lett. **18**, 426 (1993).
[12] J. H. Eberly, Q. Su, and J. Javanainen, Phys. Rev. Lett. **62**, 881 (1989); J. Opt. Soc. Am. B **6**, 1289 (1989); J. H. Eberly, Q. Su, J. Javanainen, K. C. Kulander, B. W. Shore, and L. Roso-Franco, J. Mod. Opt. **36**, 829 (1989).
[13] V. C. Reed and K. Burnett, Phys. Rev. A **42**, 3152 (1990); **43**, 6217 (1991); **46**, 424 (1992).
[14] A. Sanpera and L. Roso-Franco, Phys. Rev. A **41**, 6515 (1990); J. Opt. Soc. Am. B **8**, 1568 (1991); A. Sanpera, Q. Su, and L. Roso-Franco, Phys. Rev. A **47**, 2312 (1993).
[15] S. C. Rae and K. Burnett, Phys. Rev. A **48**, 2490 (1993).
[16] G. D. Smith, *Numerical Solution of Partial Differential Equations*, 3rd ed. (Clarendon Press, Oxford, 1985).
[17] K. Burnett, V. C. Reed, J. Cooper, and P. L. Knight, Phys. Rev. A **45**, 3347 (1992).
[18] J. L. Krause, K. J. Schafer, and K. C. Kulander, Phys. Rev. A **45**, 4998 (1992); Phys. Rev. Lett. **68**, 3535 (1992).
[19] P. B. Corkum, Phys. Rev. Lett. **71**, 1994 (1993).
[20] K. C. Kulander, K. J. Schafer, and J. L. Krause, in *Super-Intense Laser-Atom Physics*, Vol. 316 of *NATO Advanced Study Institute, Series B: Physics*, edited by B. Piraux *et al.* (Plenum Press, New York, 1993).
[21] A. L'Huillier, M. Lewenstein, P. Salières, P. Balcou, M. Ivanov, J. Larsson, and C.-G. Wahlström, Phys. Rev. A **48**, R3433 (1993).
[22] W. H. Press, B. P. Flannery, S. A. Teukolsky, and W. T. Vetterling, *Numerical Recipes* (Cambridge University Press, 1986), Sec. 12.7.
[23] S. C. Rae and K. Burnett, J. Phys. B **26**, 1509 (1993).
[24] W. M. Wood, G. Focht, and M. C. Downer, Opt. Lett. **13**, 984 (1988); M. C. Downer, W. M. Wood, and J. I. Trisnadi, Phys. Rev. Lett. **65**, 2832 (1990); W. M. Wood, C. W. Siders, and M. C. Downer, *ibid.* **67**, 3523 (1991).
[25] B. M. Penetrante, J. N. Bardsley, W. M. Wood, C. W. Siders, and M. C. Downer, J. Opt. Soc. Am. B **9**, 2032 (1992).
[26] S. P. LeBlanc, R. Sauerbrey, S. C. Rae, and K. Burnett, J. Opt. Soc. Am. B **10**, 1801 (1993).
[27] S. C. Rae and K. Burnett, Phys. Rev. A **46**, 1084 (1992); S. C. Rae, Opt. Commun. **104**, 330 (1994).